

Learning Penalty for Optimal Partitioning via Automatic Feature Extraction

Tung L Nguyen^{1*} and Toby Dylan Hocking²

¹School of Informatics, Computing, and Cyber Systems, Northern Arizona University, S San Francisco, Flagstaff, 86011, Arizona, USA.

²Département d'informatique, Université de Sherbrooke, Sherbrooke QC J1K 2R1, Quebec, Canada.

*Corresponding author(s). E-mail(s): tln229@nau.edu;
Contributing authors: toby.dylan.hocking@usherbrooke.ca;

Abstract

Changepoint detection identifies significant shifts in data sequences, making it important in areas like finance, genetics, and healthcare. The Optimal Partitioning algorithms efficiently detect these changes, using a penalty parameter to limit the changepoints count. Determining the optimal value for this penalty can be challenging. Traditionally, this process involved manually extracting statistical features, such as sequence length or variance to make the prediction. This study proposes a novel approach that uses recurrent networks to learn this penalty directly from raw sequences by automatically extracting features. Experiments conducted on 20 benchmark genomic datasets show that this novel method generally outperforms traditional ones in changepoint detection accuracy.

Keywords: changepoint detection, optimal partitioning, penalty learning, supervised machine learning, recurrent networks

1 Introduction

Changepoint detection (other words, partitioning or segmentation) is important for identifying abrupt changes in data in various domains, including finance [1], healthcare [2], network security [3], and environmental science [4]. This importance has driven the development of numerous methods over the past decades. The literature review, gap in existing methods, and study contributions are based on the diagram in Figure 1.

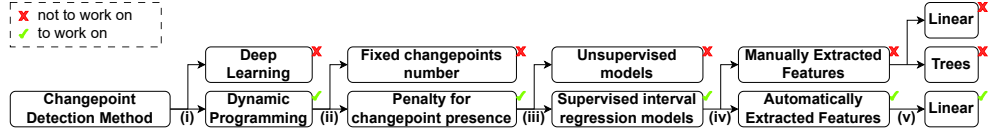


Fig. 1 Literature review of this study: (i) Selecting a detection method, (ii) Choosing a regularization method to control the changepoints number, (iii) Selecting a model type to predict the penalty, (iv) Set up the penalty prediction supervision, and (v) Choosing the model architecture.

Changepoint Detection Methods - Fig. 1 (i). The methods can be divided into Deep Learning (DL) and Dynamic Programming (DP). Pure DL and DP approaches take different perspectives. DP methods treat the problem as an optimization task, aiming to find the optimal partition, whereas DL methods frame it as a binary classification problem, predicting whether each candidate point is a changepoint. So in terms of the underlying optimization, DP methods are optimal, while DL methods are heuristic. This category division approach is similar to that of Paul Fearnhead, the author of [5] (a DP method), and [6] (a DL method) where he classifies changepoint detection methods into traditional and neural network-based. DL-based methods, which inspired from a statistical method Cumulative Sum (CUSUM) [7, 8], including recent works [6, 9] employ multilayer perceptrons (MLP) or k-nearest neighbors (KNN) as classification sliding windows to identify changepoints. However, these methods rely on local neighbors rather than the entire sequence and are overly complex for univariate data. In contrast, DP is well-suited for this context.

Regularization - Fig. 1 (ii). The DP algorithms rely on a single hyperparameter to limit the changepoints number, which can be either: (a) a fixed changepoints number or (b) a penalty parameter to penalize the changepoint presence. Fixed changepoints number allow DP algorithms [5, 10–12] to locate them, but the changepoints number is rarely predetermined. More commonly used, penalty-based DP algorithms, such as Optimal Partitioning (OPART) [13] and its variants—Pruned Exact Linear Time (PELT) [5], Functional Pruning Optimal Partitioning (FPOP) [14], and Labeled Optimal Partitioning (LOPART) [15]—are widely regarded as the most effective. PELT and FPOP prune candidate changepoints efficiently, producing identical partitions as OPART, while LOPART extends OPART by incorporating predefined labels (the expected number of changepoints within specific location ranges) or defaulting to OPART when labels are absent. OPART makes no general assumptions about the time series itself — it is simply an optimization problem:

OPART Problem. Given a sequence $\mathbf{d} \in \mathbb{R}^N$ and penalty parameter $\lambda \geq 0$, find the model parameter vector $\mathbf{m} \in \mathbb{R}^N$ that minimizes the following cost function:

$$C(\mathbf{d}, \mathbf{m}) + \lambda \sum_{i=1}^{N-1} \mathbf{1}(m_i \neq m_{i+1}),$$

where $\mathbf{1}(z)$ equals 1 when z is True and 0 otherwise. The $C(\mathbf{d}, \mathbf{m})$ formula depends on the type of change. For example, if the changes is the mean of normal distribution, then

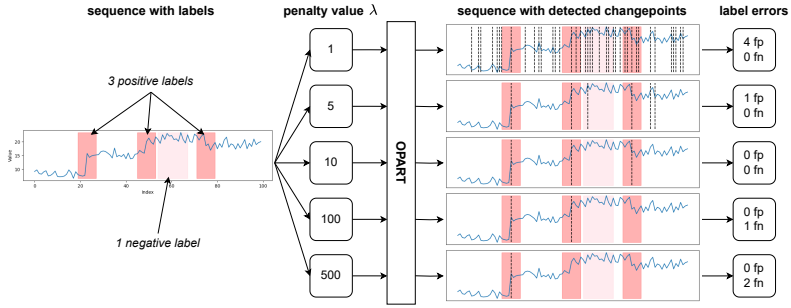


Fig. 2 Example of how λ affect the OPART changepoints. The sequence contains 4 labels: 3 positive (1 changepoint regions) and 1 negative (no changepoint region). Two types of errors are considered: false positives (fp), where extra changepoints are detected in any labels, and false negatives (fn), where no changepoint is detected in a positive label. In this example, $\lambda = 10$ is optimal.

$$C(\mathbf{d}, \mathbf{m}) = \sum_{i=1}^N (d_i - m_i)^2, \text{ or for changes in the variance, } C(\mathbf{d}, \mathbf{m}) = \sum_{i=1}^N ((d_i - m_i)^2 - \sigma_i^2)^2, \text{ where } \sigma_i^2 \text{ is the variance of the segment corresponding to } m_i.$$

In OPART algorithms, the penalty plays a key role. A higher penalty imposes a stronger penalty on changepoint presence, leading to fewer changepoints, see Figure 2. This study aims to predict that penalty to improve the changepoint detection accuracy. From here on, that conceptual penalty will be referred to as λ .

Existing λ prediction models - Fig. 1 (iii). Various models exist for predicting λ , including unsupervised [16–18] and supervised such as linear [19] and tree(s) [20–22]. But all of these models rely on a set of manually extracted sequence features, yet the number of possible features is infinite, this process can result in the inclusion of many irrelevant features, and the potential omission of useful ones.

Contribution - Fig. 1 (iv). This study proposes a novel method utilizing a recurrent network to automatically extract relevant features from sequences, which are then used to predict λ . Experiments on benchmark datasets show that the proposed method achieves higher partitioning accuracy than existing ones in most cases.

Reproducibility. To ensure transparency, the code used for this study is accessible at: https://github.com/lamtung16/ML_Changepoint_Detection_epigenomic_rnn.

2 Problem Setting and Previous Work

2.1 Problem Setting

Study supervision. Each sequence is assigned multiple *labels* indicating the expected changepoints count in a specific region, see the example in Figure 2 of a sequence having four labels.

The λ prediction models use interval regression. This study aims to predict the optimal λ for each sequence and then apply OPART with the predicted λ to detect its changepoints. For each labeled sequence, the optimal λ is *not a single value*, but rather is an *interval* $[\lambda_l, \lambda_u]$. For example, in Figure 2, $\lambda = 10$ is the optimal value, as it generates changepoints that align with expert labels; however, there exist $a, b \geq 0$ such that values of λ within $[10 - a, 10 + b]$ could produce the same result, so $[10 - a, 10 + b]$ is the *target interval* of that sequence. The algorithm for generating the target interval for each labeled sequence is detailed by Rigail et al. [19]. This problem, where the model predicts the value that falls within the target interval, is known as *interval regression*. In interval regression, there are 4 types of target intervals $[y_l, y_u]$: uncensored $[-\infty < y_l = y_u < \infty]$, interval-censored $[-\infty < y_l < y_u < \infty]$, left-censored $[-\infty = y_l < y_u < \infty]$ and right-censored $[-\infty < y_l < y_u = \infty]$. In this study, each labeled sequence is associated with an interval $[\lambda_l, \lambda_u]$ where $0 \leq \lambda_l \leq \lambda_u \leq \infty$.

2.2 Previous Work

This subsection focuses on the process of training supervised λ prediction models. Before going into the details, some noteworthy models are highlighted, which, although not applicable to this study, are still relevant. Additionally, some unsupervised models, which have served as inspiration for supervised models, are mentioned.

Noteworthy. Adaptive Linear Penalty INference (ALPIN) [23] is a method for this supervision special case, where every point is a label, equivalent to label regions having length 1. However, since this study uses a more relaxed supervision with varying label region lengths, ALPIN is not applicable.

The Accelerated Failure Time (AFT) model [24] and its variants [25–28], which are designed for censored outcomes, can be considered. Supervised changepoint detection setups involve interval-censored targets, whereas traditional AFT models are restricted to uncensored or right-censored intervals, making them not directly applicable.

Unsupervised. These models predicts λ based on some sequence features. Let $\hat{\lambda}$ denote a prediction of λ . Let N denote the sequence length, and σ its standard deviation, with examples such as Bayesian Information Criterion (BIC) [16] predicts $\hat{\lambda} = \sigma^2 \log N$. Akaike's Information Criterion (AIC) [17] predicts $\hat{\lambda} = 2p$, where p represents a sequence feature (e.g., standard deviation, variance). Lavielle [18] does not provide a closed-form formula but considers $\hat{\lambda}$ to be dependent on both N and σ .

The rest of this section will detail the training process of three supervised machine learning models: Maximum Margin Interval Regression [19], a linear model; Maximal Margin Interval Tree (MMIT) [20]; and AFT in XGBoost [21], which utilizes a tree-based framework (although AFT in XGBoost is an AFT model, it is applicable due to its ability to handle all types of non-negative intervals). These models divided the training process into 2 sequential independent steps:

- Step 1: Extract features vector \mathbf{x} from the sequence.
- Step 2: Train a model $g(\cdot)$ takes into \mathbf{x} to predict $\hat{\lambda} = g(\mathbf{x})$

2.2.1 Step 1: Feature Extraction

The manual feature extraction process, detailed in [19], involves the following steps:

- Starting from the sequence $\mathbf{d} = [d_1, d_2, \dots, d_N]$ with the mean value $\bar{d} = \frac{1}{N} \sum_{i=1}^N d_i$, 2 additional sequences (residuals and differences) are generated:

$$\begin{aligned}\mathbf{d}_{\text{res}} &= [d_1 - \bar{d}, \dots, d_N - \bar{d}] \in \mathbb{R}^N \\ \mathbf{d}_{\text{diff}} &= [d_2 - d_1, \dots, d_N - d_{N-1}] \in \mathbb{R}^{N-1}\end{aligned}$$

- Apply 3 transformations (identity, absolute, square) to each of 3 vectors, resulting in 9 transformed vectors.
- Compute 8 statistics (sum, mean, standard deviation, and quantiles at 0%, 25%, 50%, 75%, 100%) from each transformed vector, yielding a vector of length 72.
- Include the sequence length as an additional feature, forming a vector of length 73.
- Apply 5 transformations (identity, square root, log, log-log, square) to each feature, resulting in up to 365 features.

The values caused by invalid operations (e.g., log of a negative number), is ignored.

2.2.2 Step 2: Model Training

After obtaining the feature vector \mathbf{x} (up to 365 features), each instance $\{\mathbf{d}, [\lambda_l, \lambda_u]\}$ becomes $\{\mathbf{x}, [\lambda_l, \lambda_u]\}$, a selected model g is trained to predict $\hat{\lambda} = g(\mathbf{x})$.

AFT in XGBoost. The model is formulated as:

$$\hat{\lambda} = \mathbf{T}(\mathbf{x}) + \varepsilon$$

Here, $\mathbf{T}(\mathbf{x})$ denotes the ensemble of trees for feature vector \mathbf{x} , and ε is a random error. The model is trained by minimizing the negative log-likelihood over all train instances:

$$l_{AFT}(\hat{\lambda}, [\lambda_l, \lambda_u]) = -\log \left[F_Z\left(\frac{\lambda_u - \hat{\lambda}}{\sigma}\right) - F_Z\left(\frac{\lambda_l - \hat{\lambda}}{\sigma}\right) \right] \quad (1)$$

where $\sigma > 0$ is the scale parameter. The cumulative distribution function $F_Z(z)$ depends on the chosen distribution of ε :

- normal: $F_Z(z) = \frac{1}{2}(1 + \text{erf}(\frac{z}{\sqrt{2}}))$
- logistic: $F_Z(z) = \frac{e^z}{1+e^z}$
- extreme: $F_Z(z) = 1 - e^{-\exp z}$

The model is trained using the gradient boosting algorithm [29] to minimize the loss value (1) over the training dataset with S instances $\{\mathbf{x}^i, [\lambda_l^i, \lambda_u^i]\}_{i=1}^S$ given the

distribution of ε and the scale parameter σ :

$$\sum_{i=1}^S l_{AFT}\left(\hat{\lambda}^i, [\log \lambda_l^i, \log \lambda_u^i]\right) = -\sum_{i=1}^S \log \left[F_Z\left(\frac{\lambda_u^i - \mathbf{T}(\mathbf{x}^i)}{\sigma}\right) - F_Z\left(\frac{\lambda_l^i - \mathbf{T}(\mathbf{x}^i)}{\sigma}\right) \right]$$

Linear. This model, known as Maximum Margin Interval Regression, transforms the problem to predicting $\log \hat{\lambda}$ instead of $\hat{\lambda}$, as $\log \hat{\lambda}$ can be any real value, unlike the non-negative $\hat{\lambda}$. The model expresses the output as a linear combination of inputs:

$$\log \hat{\lambda} = \mathbf{x} \cdot \beta + \beta_0 \quad (2)$$

where β is the parameter vector, $\mathbf{x} \cdot \beta$ is the dot product of \mathbf{x} and β , and β_0 is the bias term. Its simplified version, used in [15], predicts $\log \hat{\lambda} = \beta_1 \times \log \log N + \beta_0$, where N is the sequence length.

This model is trained by minimizing a loss function, the Hinge Error, defined by Rigaill et al. [19], it achieves 0 loss when the prediction falls within the target interval. The error value between prediction $\log \hat{\lambda}$ and target interval $[\log \lambda_l, \log \lambda_u]$ is:

$$l\left(\log \hat{\lambda}, [\log \lambda_l, \log \lambda_u]\right) = \begin{cases} (\log \lambda_l - \log \hat{\lambda} + \epsilon)^2 & \text{if } \log \hat{\lambda} < \log \lambda_l + \epsilon, \\ 0 & \text{if } \log \lambda_l + \epsilon \leq \log \hat{\lambda} \leq \log \lambda_u - \epsilon, \\ (\log \hat{\lambda} - \log \lambda_u + \epsilon)^2 & \text{if } \log \hat{\lambda} > \log \lambda_u - \epsilon. \end{cases}$$

where $\epsilon \geq 0$ is the margin length ($\epsilon = 0$ by default). The Hinge Error becomes Square Error when $\lambda_l = \lambda_u$ and $\epsilon = 0$ (or $\epsilon = \frac{\log \lambda_l + \log \lambda_u}{2}$), or in other word, target interval becomes target point. Drouin et al. [20] proposed a similar loss function:

$$l\left(\log \hat{\lambda}, [\log \lambda_l, \log \lambda_u]\right) = \begin{cases} |\log \lambda_l - \log \hat{\lambda} + \epsilon| & \text{if } \log \hat{\lambda} < \log \lambda_l + \epsilon, \\ 0 & \text{if } \log \lambda_l + \epsilon \leq \log \hat{\lambda} \leq \log \lambda_u - \epsilon, \\ |\log \hat{\lambda} - \log \lambda_u + \epsilon| & \text{if } \log \hat{\lambda} > \log \lambda_u - \epsilon. \end{cases}$$

Using the ReLU function, the general loss function can be written in this short form:

$$l(\log \hat{\lambda}, [\log \lambda_l, \log \lambda_u]) = \left(\text{ReLU}(\log \lambda_l - \log \hat{\lambda} + \epsilon) \right)^p + \left(\text{ReLU}(\log \hat{\lambda} - \log \lambda_u + \epsilon) \right)^p, \quad (3)$$

where $\epsilon \geq 0$ is the margin length and $p \in \{1, 2\}$ is the loss type.

To estimate the parameters β and β_0 in (2), the Fast Iterative Shrinkage-Thresholding Algorithm (FISTA) [30] with respect to β and β_0 is employed to minimize the Hinge Error (3) over the train dataset having S instances $\{\mathbf{x}^i, [\log \lambda_l^i, \log \lambda_u^i]\}_{i=1}^S$:

$$\sum_{i=1}^S l\left(\log \hat{\lambda}^i, [\log \lambda_l^i, \log \lambda_u^i]\right) = \sum_{i=1}^S l\left(\mathbf{x}^i \cdot \beta + \beta_0, [\log \lambda_l^i, \log \lambda_u^i]\right)$$

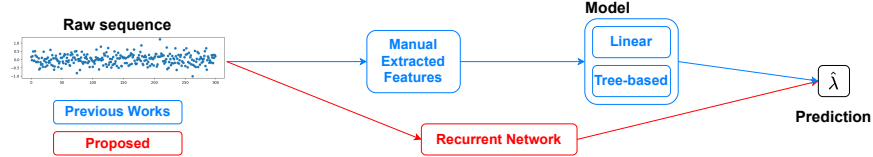


Fig. 3 Diagram of the methods - Instead of performing feature extraction and the learning model separately, the proposed method uses a recurrent network to combine both into a single operation.

Tree. MMIT introduced by Drouin et al. [20] is applicable for λ prediction as an interval regression model. The MMIT model is:

$$\log \hat{\lambda} = \mathcal{T}(\mathbf{x})$$

The tree \mathcal{T} architecture follows the same structure as CART (Classification And Regression Tree) [31]. The only difference lies in the regression value for each leaf which is a set of Q instances $\{\mathbf{x}^i, [\log \lambda_l^i, \log \lambda_u^i]\}_{i=1}^Q$: instead of taking the mean of all targets like CART does, MMIT chooses a constant value c that minimizes the mean Hinge Error (3) between this constant and the target intervals:

$$\operatorname{argmin}_c \frac{1}{Q} \sum_{i=1}^Q l(c, [\log \lambda_l^i, \log \lambda_u^i]), \quad c \in \mathbf{R}$$

A heuristic algorithm is used to speed up the estimation of the mean value for each leaf by considering a finite set of candidates, rather than solving for the optimal c :

$$\operatorname{argmin}_c \frac{1}{Q} \sum_{i=1}^Q l(c, [\log \lambda_l^i, \log \lambda_u^i]),$$

where $c \in \{\log \lambda_l^i, \log \lambda_u^i, \frac{\log \lambda_l^i + \log \lambda_u^i}{2} \mid \log \lambda_l^i > -\infty, \log \lambda_u^i < \infty\}_{i=1}^Q$

The training procedure for determining the optimal tree architecture follows the same operations as in CART (binary optimization) to minimize the Hinge Error (3) over the train dataset having S instances $\{\mathbf{x}^i, [\log \lambda_l^i, \log \lambda_u^i]\}_{i=1}^S$:

$$\sum_{i=1}^S l(\log \hat{\lambda}^i, [\log \lambda_l^i, \log \lambda_u^i]) = \sum_{i=1}^S l(\mathcal{T}(\mathbf{x}^i), [\log \lambda_l^i, \log \lambda_u^i])$$

3 Novelty

In previous work, the prediction of λ involves two independent steps. In step 1, which manually extracts sequence features, redundancy may be introduced, and important

sequence feature	k	m	h_{k-1}	h_t	used in
length	$k \in \mathbf{N}^+$	1	$k-1$	$h_{t-1} + 1$	[15–21, 32]
mean	1	1	0	$h_{t-1} + \frac{d_t - h_{t-1}}{t}$	[19–21]
min	1	1	∞	$\min(d_t, h_{t-1})$	[19–21]
max	1	1	$-\infty$	$\max(d_t, h_{t-1})$	[19–21]
sum	1	1	0	$h_{t-1} + d_t$	[19–21]
cumulative absolute	1	1	0	$h_{t-1} + d_t $	[19–21]
cumulative squares	1	1	0	$h_{t-1} + d_t^2$	[19–21]
difference sum	2	1	0	$ d_t - d_{t-1} + h_{t-1}$	[19–21, 32]
value range	1	2	∞ $-\infty$	$\min(d_t, h_{t-1}^{(1)})$ $\max(d_t, h_{t-1}^{(2)})$	[19–21, 32]

Table 1 Formula of recurrent core for each feature approximation.

hidden features may be missed. To address this, we propose a model that combines both steps into one, utilizing a recurrent network to automatically extract relevant features from the raw sequence to predict λ , see Figure 3.

Feature Extraction via Recurrent Networks. In a Recurrent Network with input size $k \geq 1$ and hidden size $m \geq 1$, processing a sequence $\mathbf{d} = [d_1, d_2, \dots, d_N] \in \mathbb{R}^N$, the hidden state at time t , called h_t , using a function f , is updated as:

$$h_t = f(d_{[t-k+1:t]}; h_{t-1}) \in \mathbb{R}^m \quad (4)$$

where $d_{[t-k+1:t]} = [d_{t-k+1}, d_{t-k+2}, \dots, d_t] \in \mathbb{R}^k$. Time stamp t ranges from k to N . The initial hidden state h_{k-1} can be assigned manually. The final hidden state $h_N \in \mathbb{R}^m$ captures information from the entire sequence. Thus, we use h_N as the *m automatically extracted features* from the raw sequence.

λ prediction. The prediction is the linear combination of m extracted features:

$$\log \hat{\lambda} = h_N \cdot \beta + \beta_0 \quad \text{or} \quad \hat{\lambda} = e^{h_N \cdot \beta + \beta_0}$$

where $\beta \in \mathbb{R}^m$ and $\beta_0 \in \mathbb{R}$ are the parameters to be learned.

Feature Approximation Ability of Recurrent Networks. Recurrent networks have the ability to approximate sequence features. The core component of these models is a neural network. For instance, the Vanilla Recurrent Network [33] core is a fully connected neural network, which, according to the universal approximation theorem [34], can approximate any continuous function, regardless of its complexity, provided there are enough neurons in the hidden layer. This is why, although these models

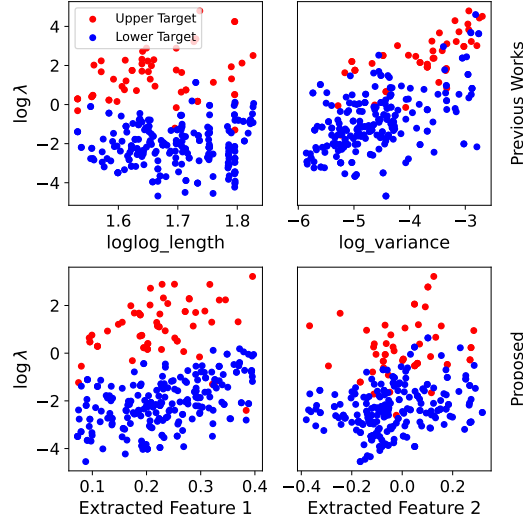


Fig. 4 Example: features vs. targets from the dataset detailed. The upper plots: the length or variance vs. targets, as these features are used on λ prediction unsupervised methods. The lower plots: automatically extracted features vs targets, using a GRU model with two extracted features. Since we consider the predicted λ has a linear relationship with the features, a good feature should exhibit a fairly linear pattern in the plot.

may not directly produce exact statistical sequence features, their architecture enables them to approximate these features with a high degree of accuracy. Refer to Table 1 to see how recurrent networks are capable of approximating sequence features.

Automatic vs. Manual extracted features. Figure 4 provides an example by comparing the ability to predict λ using length (or variance) - as these features are considered key for λ prediction in unsupervised methods - versus automatic extracted features from recurrent networks. Since we assume that the predicted value of λ has a linear relationship with the features, a good feature should display a linear pattern in the plot. It can be seen that the automatically extracted Feature 1 exhibits an excellent linear pattern with the all the target intervals since it's easy to visualize a line intersecting most of these intervals.

Recurrent network architectures. This study explores 3 recurrent networks: Vanilla Recurrent Network (RNN), Long Short-Term Memory (LSTM) [35], Gated Recurrent Unit (GRU) [36]. RNNs struggle with long-term dependencies due to the vanishing gradient problem. LSTMs address this by using memory cells and gating mechanisms that help retain information over longer sequences. GRUs, a simplified version of LSTMs, combine the forget and input gates into a single update gate, offering a more efficient alternative while still capturing long-term dependencies.

Table 2 List of datasets with its number of sequences (Size)

Dataset	Seq. length	Size	Source
systematic	66 - 5937	3418	
detailed	25 - 5937	3730	GitHub
cancer	39 - 43628	826	
ATAC_JV_adipose	105716 - 11.50M	465	
CTCF_TDH_ENCODE	166431 - 11.09M	182	
H3K27ac-H3K4me3_TDHAM_BP	275 - 4.33M	2008	
H3K27ac_TDH_some	41053 - 6.74M	95	
H3K27me3_RL_cancer	5730 - 1.89M	171	
H3K27me3_TDH_some	113523 - 3.00M	43	
H3K36me3_AM_immune	184092 - 7.14M	420	
H3K36me3_TDH_ENCODE	68209 - 2.74M	78	
H3K36me3_TDH_immune	434882 - 4.35M	37	UCI Repo
H3K36me3_TDH_other	49362 - 7.15M	40	
H3K4me1_TDH_BP	148275 - 9.73M	144	
H3K4me3_PGP_immune	24460 - 6.62M	297	
H3K4me3_TDH_ENCODE	18198 - 7.21M	75	
H3K4me3_TDH_immune	87557 - 7.81M	378	
H3K4me3_TDH_other	80674 - 3.72M	90	
H3K4me3_XJ_immune	52498 - 5.50M	270	
H3K9me3_TDH_BP	369654 - 10.29M	120	

4 Experiments

In this section, the implementation of models is detailed. Labeled sequences are first processed, with features manually extracted to replicate previous work, along with the corresponding target intervals. Baseline models and the proposed models are then implemented. For each test sequence, OPART is applied with the predicted λ to detect changepoints. Finally, accuracy rates are calculated based on the predicted changepoints and the test set labels.

Raw Sequence Datasets. This study uses 20 datasets: two DNA copy number profiles from neuroblastoma tumors [19], known for detailed and systematic dataset; one dataset cancer from [15]; and 17 ChIP-seq datasets from [37], see Table 2 for all benchmark datasets, each sequence has a different length (number of datapoints), so the range of sequence lengths within each dataset is reported in the Table 2. For each sequence in each dataset, biologist experts use their visual interpretation of important signal and noise patterns to label regions as having changes in mean value or not.

Train/Test Setup. Each sequence is assigned a unique identifier (sequenceID), and datasets are split into folds based on these IDs. Fewer folds are used for smaller datasets to balance train and test data sizes, ensuring a sufficiently large test set for

Table 3 List of employed models

Model	Regularization	Language	Package	Paper
linear	L1	R	[38]	[19]
MMIT	tree architecture	Python/Cpp binding	[39]	[20]
AFT_XGboost	tree architecture	Python	[40]	[21]
constant	none	Python/Cpp binding	[39]	Baseline
MLP	hidden layer number hidden layer sizes	Python		Additional
RNN LSTM GRU	hidden layer number hidden state sizes	Python		Proposed

reliable evaluation. In each iteration, one fold serves as the test set, and the others form the train set.

Evaluation Metrics. The metric used is the accuracy rate on the test set:

$$\text{Accuracy} = \frac{TP + TN}{TP + TN + FP + FN}$$

where

- TP = True Positives (The number of detected changepoints matches to the positive labels)
- TN = True Negatives (No detected changepoints in the negative labels)
- FP = False Positives (The number of detected changepoints exceeds that of the labels.)
- FN = False Negatives (The number of detected changepoints is less than that of the labels.)

4.1 Model Implementation

Previous models were implemented as baselines, along with additional models and the proposed models for comparison. Details of all models are provided in Table 3.

4.1.1 Baseline Models

Linear. This model uses L1 regularization. The regularization parameter L1 starts at 0.001, geometrically increasing by a factor of 1.2 until no features remain, with cross-validation determining the optimal L1 regularization value.

MMIT. The optimal hyperparameters are chosen through cross-validation on the train training set, including:

- `max_depth`: values of 0, 1, 5, 10, 20, and ∞
- `min_sample`: values of 0, 1, 2, 4, 8, 16, and 20.

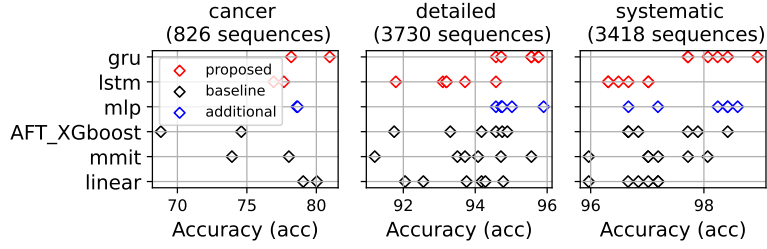


Fig. 5 The accuracies for each fold are presented for datasets without any pooling preprocessing. The cancer dataset has 2 folds, while the other two datasets each have 6 folds. The Constant and RNN models have been excluded due to their small accuracies to better highlight the differences and improve visualization. Overall, the GRU model achieves the highest accuracy.

- `margin` (ϵ in Hinge Error 3): values of 0, 1, and 2
- `loss_type`: values of `hinge` and `square` (equivalent to $p = 1$ and $p = 2$ in Hinge Error 3);

AFT in XGBoost. Following the same setup described in Barnwal et al. [21], the optimal hyperparameters are chosen through cross-validation on the train training set, including:

- `learning_rate`: 0.001, 0.01, 0.1, and 1.0
- `max_depth`: 2, 3, 4, 5, 6, 7, 8, 9, and 10
- `min_child_weight`: 0.001, 0.1, 1.0, 10.0, and 100.0
- `reg_alpha`: 0.001, 0.01, 0.1, 1.0, 10.0, and 100.0
- `reg_lambda`: 0.001, 0.01, 0.1, 1.0, 10.0, and 100.0
- `aft_loss_distribution_scale`: 0.5, 0.8, 1.1, 1.4, 1.7, and 2.0

Constant (Featureless). This model predicts a single value $\hat{\lambda} = \exp \log \hat{\lambda}$ from the train set using only target intervals. The objective is to minimize the total Hinge Error (3) over S instances with target intervals $[\log \lambda_l^i, \log \lambda_u^i]_{i=1}^S$:

$$\log \hat{\lambda} = \operatorname{argmin}_c \sum_{i=1}^S l(c, [\log \lambda_l^i, \log \lambda_u^i]).$$

4.1.2 Additional Model

MLP. Using the same feature vector and loss function as the linear model, the MLP generalizes the linear model by incorporating ReLU activation in the hidden layers. Hyperparameters include the number of hidden layers (1, 2, or 3) and the size of each hidden layer (1, 2, 4, 8, 16, 32, 64, 128, 256, or 512). The best hyperparameters are chosen via cross-validation in the train set. Since the linear model uses L1 regularization

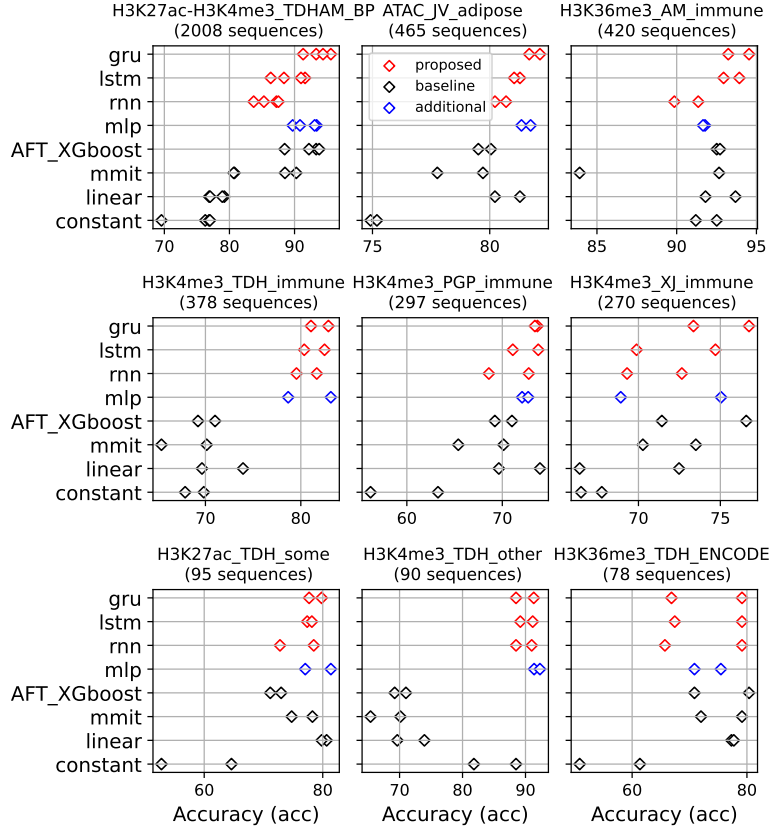


Fig. 6 The fold accuracies on some ChIP-seq datasets are presented, with the datasets ordered from largest to smallest. The number of colored diamonds in any row represents the number of folds for each dataset. As observed, for larger datasets, more complex models tend to show higher accuracy. For the last three smaller datasets, recurrent networks do not always outperform the previous methods.

and MMIT (or AFT in XGBoost) has a tree-based architecture, they can automatically select features. However, MLP does not fully mitigate irrelevant features on its own (parameters associated with each feature are likely non-zero). Feature selection for MLP in this interval regression setting could be explored in future work.

4.1.3 Proposed Models

Architecture. There are three considered models: RNN, LSTM, and GRU. The hyperparameters include: the number of hidden layers (1 or 2) and the hidden state size (number of extracted features) (2, 4, 8 or 16).

Preprocessing. Based on the sequence lengths of 20 datasets, we handle them as follows:

- For the 3 datasets—detailed, systematic, cancer—the sequence lengths range from 39 to 43628. These sequences are directly input into the λ prediction models without further modification.
- For the 17 ChIP-seq datasets, the sequence lengths can be over 11 million. Training on these raw sequences can be computationally expensive and time-consuming. So pooling operations are performed, where a single representative value is chosen for each non-overlapping sliding window. The window size options are 100, 1000, or 2000, and the representative value is either the window mean or the median. After shortening the sequences, a $\log(z + 1)$ transformation is applied to all value z in all shortened sequences to mitigate skewed distributions. Following this, all sequence values are normalized (mean 0, variance 1) for each dataset.

4.2 Results

The comprehensive accuracy results of all 8 methods for each of 20 datasets are provided in the Appendix, as the table is too large to be included in the main paper. Figure 5 presents the accuracy rates for three datasets using the original, unpooled sequences, while Figure 6 shows the results for various ChIP-seq datasets (pooled sequences). Each dataset is evaluated using seven different methods, producing multiple accuracy values depending on the number of folds used for that dataset.

5 Discussion and Conclusion

Summary of Contributions. Technically, these proposed models still perform two steps: (1) Feature extraction and (2) Predicting λ based on the extracted features. However, instead of performing these steps separately, it combines them into a single operation, enhancing its robustness compared to previous models. Automatic extracting features helps generate highly useful ones without requiring many features, as shown in Figure 4. This study focuses exclusively on genomic datasets, where prior knowledge of relevant features enables effective manual feature extraction. However, the proposed models stand out because it does not require expert knowledge to perform. Its automatic feature extraction mechanism makes it versatile and applicable to any type of sequence dataset.

Comparison to Previous Models. Recurrent networks, in general, outperform previous models across datasets, see Figure 5 and Figure 6. For small datasets (with fewer than 100 instances), the accuracy of the proposed models is comparable (neither better nor worse) to that of existing models. On the other hand, when dealing with larger datasets, recurrent networks noticeably outperform previous models and show a slight edge over MLPs.

Comparison between Recurrent Networks. When comparing RNN, LSTM, and GRU, as expected, RNN performs the worst due to its difficulty with long-term memory. In most cases, GRU outperforms the others.

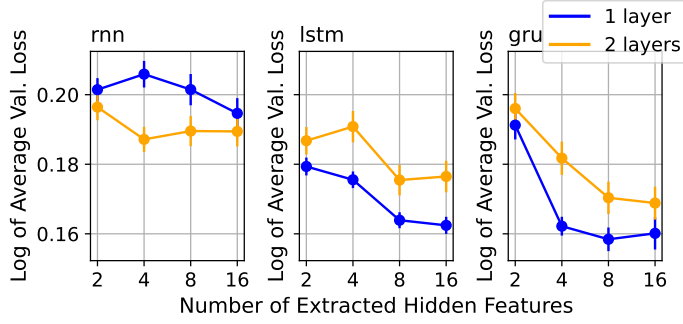


Fig. 7 Log of the loss validation with 68.27% confidence interval across different numbers of extracted hidden layers in the three proposed models shows that the number of extracted hidden features needs to be sufficient. As seen in the figure, when the number of features is 8 or 16, the loss value is lower compared to when the number of features is 2 or 4.

Discussion on the Number of Automatic Extracted Features. As shown in the Figure 7, the number of automatic extracted features needs to be sufficiently large. It is observed that when 8 or 16 features are extracted, the validation loss value is slightly smaller compared to when only 2 or 4 features are extracted.

Impact of pooling preprocessing. Figure 8 shows that shortening the sequence for training is effective. As the window size increases, more information is lost. However, when the window size is small, such as 100, the performance of the recurrent models is worse compared to larger window sizes like 1000 or 2000. This could be because the pooled sequence with a window size of 100 is still too long for the recurrent models to handle effectively. The pooling process is beneficial in two ways: it can improve the accuracy of recurrent networks and also reduce training time. We employed two pooling functions, mean and median, to represent a single value for each non-overlapping window. As shown in Figure 8, it is evident that using the mean value as the representation consistently yields smaller loss.

Study Limitations. Although the Recurrent Network architecture is straightforward, as its core essentially a deep neural network, training these models can be time-consuming due to the inherently sequential nature of the process. For some train/test pairs, even after applying pooling to reduce the sequence length, training a model with a maximum of 2 layers, each containing no more than 16 neurons, and a maximum of 1000 iterations, took over approximately 10 days, despite utilizing the powerful NVIDIA A100 GPU. These models also require significant memory to store the hidden states at each time step. To avoid out-of-memory (OOM) errors, it is crucial to allocate sufficient memory, especially for long sequences.

Practical Considerations in Real-World Applications. There is a trade-off between training time and accuracy. The proposed models have higher accuracy in

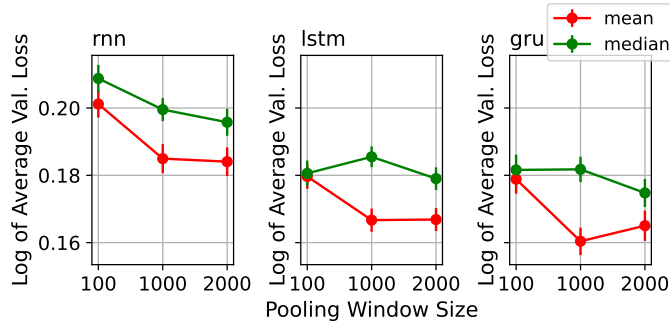


Fig. 8 Log of the loss validation with 68.27% confidence interval across different pooling methods in the three proposed models reveals that the window size must be large enough to reduce training time and difficulty, yet small enough to retain crucial information. The figure shows that mean pooling outperforms median pooling. These results are based on 17 ChIP-seq datasets.

most of the 20 datasets, but they are significantly more time-consuming to train, especially for longer sequences. In contrast, manual extracted features models do not face this issue. Therefore, in real-world scenarios where datasets contain only a few sequences but each sequence is long, and training time is a priority, manual extracted features models may be the better choice for two reasons: first, their training time is significantly faster; and second, these models' accuracy is comparable to the proposed models, which can be seen in the bottom three panels of Figure 6. However, if the user's priority is accuracy and the hardware requirements are met, the proposed models are a better choice. Although the training process is time-consuming, it only needs to be done once; afterwards, the trained models can be applied to unseen sequences, as their feed-forward process is sufficiently fast.

Future Directions. For these particular datasets, it is assumed that λ exhibits an increasingly monotonic behavior with respect to both sequence length and variance, which are employed in unsupervised methods. One approach is to leverage monotonic network architectures, such as min-max networks [41], or more advanced architectures like Lattice Networks [42], with modifications to the loss function for each linear region.

We can consider CNNs [43] because they are capable of handling sequences of varying lengths and generating a single output by utilizing convolution layers to extract features across the sequence. Global pooling layers (e.g., Global Max or Average Pooling) aggregate these features into a fixed-size representation. This vector is then passed through a MLP to produce the final output.

To build upon the initial concept of utilizing recurrent networks in this study, various types of models could be explored in the future:

- Using a more complex model: This study predicts λ by using a linear combination of the extracted features. Alternatively, we could consider using a more complex model such as MLP that processes the extracted features instead of relying on a linear combination.

- Attention mechanisms [44] dynamically focus on relevant input parts, assigning importance weights to subsequences. Unlike sequential RNNs, they effectively capture long-range dependencies and handle varying input lengths, making them ideal for this task.
- Bidirectional Recurrent Networks [45]: The models implemented in this study are unidirectional, leading to challenges with long-term memory, since the later parts of the sequence tend to be more important than the earlier ones. Using a bidirectional recurrent network architecture can aim to address this limitation, enabling the model to better capture information from the sequence.

Funding sources

This research did not receive any specific grant from funding agencies in the public, commercial, or not-for-profit sectors.

References

- [1] Lattanzi, C., Leonelli, M.: A change-point approach for the identification of financial extreme regimes. *Brazilian Journal of Probability and Statistics* **35**(4) (2021) <https://doi.org/10.1214/21-bjps509>
- [2] Muggeo, V.M.R., Adelfio, G.: Efficient change point detection for genomic sequences of continuous measurements. *Bioinformatics* **27**(2), 161–166 (2010) <https://doi.org/10.1093/bioinformatics/btq647>
- [3] Tartakovsky, A.G., Polunchenko, A.S., Sokolov, G.: Efficient computer network anomaly detection by changepoint detection methods. *IEEE Journal of Selected Topics in Signal Processing* **7**(1), 4–11 (2013) <https://doi.org/10.1109/JSTSP.2012.2233713>
- [4] Reeves, J., Chen, J., Wang, X.L., Lund, R., Lu, Q.Q.: A review and comparison of changepoint detection techniques for climate data. *Journal of Applied Meteorology and Climatology* **46**(6), 900–915 (2007) <https://doi.org/10.1175/jam2493.1>
- [5] Killick, R., Fearnhead, P., Eckley, I.A.: Optimal detection of changepoints with a linear computational cost. *Journal of the American Statistical Association* **107**(500), 1590–1598 (2012)
- [6] Li, J., Fearnhead, P., Fryzlewicz, P., Wang, T.: Automatic change-point detection in time series via deep learning. *Journal of the Royal Statistical Society Series B: Statistical Methodology* **86**(2), 273–285 (2024)
- [7] Hinkley, D.V.: Inference about the change-point from cumulative sum tests. *Biometrika* **58**(3), 509–523 (1971)
- [8] James, B., James, K.L., Siegmund, D.: Tests for a change-point. *Biometrika* **74**(1), 71–83 (1987)
- [9] Ermshaus, A., Schäfer, P., Leser, U.: Clasp: parameter-free time series segmentation. *Data Mining and Knowledge Discovery* **37**(3), 1262–1300 (2023)
- [10] Auger, I.E., Lawrence, C.E.: Algorithms for the optimal identification of segment neighborhoods. *Bulletin of mathematical biology* **51**(1), 39–54 (1989)
- [11] Bai, J., Perron, P.: Computation and analysis of multiple structural change models. *Journal of applied econometrics* **18**(1), 1–22 (2003)
- [12] Rigail, G.: A pruned dynamic programming algorithm to recover the best segmentations with 1 to k {max} change-points. *Journal de la Société Française de Statistique* **156**(4), 180–205 (2015)

- [13] Jackson, B., Scargle, J.D., Barnes, D., Arabhi, S., Alt, A., Gioumousis, P., Gwin, E., Sangtrakulcharoen, P., Tan, L., Tsai, T.T.: An algorithm for optimal partitioning of data on an interval. *IEEE Signal Processing Letters* **12**(2), 105–108 (2005)
- [14] Maidstone, R., Hocking, T., Rigaill, G., Fearnhead, P.: On optimal multiple changepoint algorithms for large data. *Statistics and Computing* **27**(2), 519–533 (2016) <https://doi.org/10.1007/s11222-016-9636-3>
- [15] Hocking, T.D., Srivastava, A.: Labeled optimal partitioning. *Computational Statistics* **38**(1), 461–480 (2023) <https://doi.org/10.1007/s00180-022-01238-z>
- [16] Schwarz, G.: Estimating the Dimension of a Model. *The Annals of Statistics* **6**(2), 461–464 (1978) <https://doi.org/10.1214/aos/1176344136>
- [17] Akaike, H.: A new look at the statistical model identification. *IEEE transactions on automatic control* **19**(6), 716–723 (1974)
- [18] Lavielle, M.: Using penalized contrasts for the change-point problem. *Signal Processing* **85**(8), 1501–1510 (2005) <https://doi.org/10.1016/j.sigpro.2005.01.012>
- [19] Rigaill, G., Hocking, T.D., Bach, F., Vert, J.-P.: Learning Sparse Penalties for Change-Point Detection using Max Margin Interval Regression (2013). <https://inria.hal.science/hal-00824075> Accessed 2024-01-10
- [20] Drouin, A., Hocking, T.D., Laviolette, F.: Maximum margin interval trees. In: *Proceedings of the 31st International Conference on Neural Information Processing Systems. NIPS’17*, pp. 4954–4963. Curran Associates Inc., Red Hook, NY, USA (2017)
- [21] Barnwal, A., Cho, H., Hocking, T.: Survival regression with accelerated failure time model in xgboost. *Journal of Computational and Graphical Statistics* **31**(4), 1292–1302 (2022)
- [22] Nguyen, T.L., Hocking, T.D.: Interval Regression: A Comparative Study with Proposed Models (2025). <https://arxiv.org/abs/2503.02011>
- [23] Truong, C., Gudre, L., Vayatis, N.: Penalty learning for changepoint detection. In: *2017 25th European Signal Processing Conference (EUSIPCO)*, pp. 1569–1573 (2017). <https://doi.org/10.23919/EUSIPCO.2017.8081473>
- [24] Wei, L.-J.: The accelerated failure time model: a useful alternative to the cox regression model in survival analysis. *Statistics in medicine* **11**(14-15), 1871–1879 (1992)
- [25] Cai, T., Huang, J., Tian, L.: Regularized estimation for the accelerated failure time model. *Biometrics* **65**(2), 394–404 (2009)

- [26] Huang, J., Ma, S., Xie, H.: Regularized estimation in the accelerated failure time model with high-dimensional covariates. *Biometrics* **62**(3), 813–820 (2006)
- [27] Quinlan, J.R.: Induction of decision trees. *Machine learning* **1**, 81–106 (1986)
- [28] Pölsterl, S., Navab, N., Katouzian, A.: An efficient training algorithm for kernel survival support vector machines. *arXiv preprint arXiv:1611.07054* (2016)
- [29] Friedman, J.H.: Greedy function approximation: A gradient boosting machine. *The Annals of Statistics* **29**(5), 1189–1232 (2001). Accessed 2025-08-26
- [30] Chambolle, A., Dossal, C.H.: On the convergence of the iterates of “fista”. *Journal of Optimization Theory and Applications* **166**(3), 25 (2015)
- [31] Breiman, L., Friedman, J.H., Olshen, R.A., Stone, C.: Classification and regression trees (cart). *Biometrics* **40**(3), 358 (1984)
- [32] Nguyen, T.L., Hocking, T.D.: Penalty learning for optimal partitioning using multilayer perceptron. *Statistics and Computing* **35**(5) (2025) <https://doi.org/10.1007/s11222-025-10680-0>
- [33] Rumelhart, D.E., Hinton, G.E., Williams, R.J.: Learning representations by back-propagating errors. *nature* **323**(6088), 533–536 (1986)
- [34] Hornik, K., Stinchcombe, M., White, H.: Multilayer feedforward networks are universal approximators. *Neural networks* **2**(5), 359–366 (1989)
- [35] Hochreiter, S.: Long short-term memory. *Neural Computation* MIT-Press (1997)
- [36] Chung, J., Gulcehre, C., Cho, K., Bengio, Y.: Empirical evaluation of gated recurrent neural networks on sequence modeling. *arXiv preprint arXiv:1412.3555* (2014)
- [37] Hocking, T.D., Goerner-Potvin, P., Morin, A., Shao, X., Pastinen, T., Bourque, G.: Optimizing ChIP-seq peak detectors using visual labels and supervised machine learning. *Bioinformatics* **33**(4), 491–499 (2016) <https://doi.org/10.1093/bioinformatics/btw672>
- [38] Hocking, T.D.: *penaltyLearning: Penalty Learning.* (2024). R package version 2024.1.25. <https://github.com/tdhock/penaltylearning>
- [39] Drouin: Maximum Margin Interval Trees. (2017). <https://github.com/aldo61/mmit>
- [40] Chen, T., He, T., Benesty, M., Khotilovich, V., Tang, Y., Cho, H., Chen, K., Mitchell, R., Cano, I., Zhou, T., Li, M., Xie, J., Lin, M., Geng, Y., Li, Y., Yuan, J., Cortes, D.: Xgboost: Extreme Gradient Boosting. (2025). R package version 3.2.0.0. <https://github.com/dmlc/xgboost>

- [41] Sill, J.: Monotonic networks. *Advances in neural information processing systems* **10** (1997)
- [42] You, S., Ding, D., Canini, K., Pfeifer, J., Gupta, M.: Deep lattice networks and partial monotonic functions. In: Guyon, I., Luxburg, U.V., Bengio, S., Wallach, H., Fergus, R., Vishwanathan, S., Garnett, R. (eds.) *Advances in Neural Information Processing Systems*, vol. 30. Curran Associates, Inc., ??? (2017)
- [43] LeCun, Y., Bottou, L., Bengio, Y., Haffner, P.: Gradient-based learning applied to document recognition. *Proceedings of the IEEE* **86**(11), 2278–2324 (1998)
- [44] Bahdanau, D., Cho, K., Bengio, Y.: Neural machine translation by jointly learning to align and translate. *CoRR* **abs/1409.0473** (2014)
- [45] Schuster, M., Paliwal, K.K.: Bidirectional recurrent neural networks. *IEEE transactions on Signal Processing* **45**(11), 2673–2681 (1997)

Appendix

Table 4 Accuracy means and standard deviations (by method)

	Dataset	constant	linear	nnmit	AFT-XGB	mlp	rnn	lstm	gru
cancer		63.37 ± 14.93	79.55 ± 0.70	75.97 ± 2.90	71.70 ± 4.10	78.62 ± 0.04	75.42 ± 2.12	77.29 ± 0.52	79.58 ± 1.96
cellular		67.45 ± 6.42	93.60 ± 1.07	93.80 ± 1.47	93.91 ± 1.20	94.95 ± 0.49	86.26 ± 4.64	93.26 ± 0.91	95.32 ± 0.53
systematic		56.87 ± 9.87	96.81 ± 0.46	97.16 ± 0.72	97.37 ± 0.75	97.92 ± 0.80	72.87 ± 29.01	96.64 ± 0.32	98.19 ± 0.47
ATAC-JV.adipose		75.05 ± 0.19	80.75 ± 0.75	78.74 ± 1.38	79.78 ± 0.38	81.55 ± 0.28	80.46 ± 0.33	81.16 ± 0.17	81.91 ± 0.32
CTCF-TDH_ENCODE		75.47 ± 1.71	84.15 ± 0.40	87.65 ± 0.54	93.32 ± 0.84	93.96 ± 0.38	86.58 ± 0.23	89.97 ± 2.50	91.52 ± 7.80
H3K27ac-H3K4me3_TDHAM_BP		74.93 ± 3.60	78.00 ± 1.22	85.06 ± 5.06	91.95 ± 2.41	91.76 ± 1.77	85.94 ± 1.78	89.33 ± 2.44	93.65 ± 1.80
H3K27ac.TDH.some		58.69 ± 8.35	80.23 ± 0.60	76.51 ± 2.48	72.06 ± 1.30	79.21 ± 3.05	75.63 ± 4.03	77.77 ± 0.56	78.76 ± 1.49
H3K27me3_RL.cancer		54.86 ± 1.35	64.52 ± 5.54	65.90 ± 2.32	65.23 ± 0.78	67.58 ± 3.57	64.43 ± 3.32	65.49 ± 3.24	64.22 ± 4.08
H3K27me3_TDH.some		62.19 ± 2.89	85.48 ± 1.90	77.19 ± 6.68	85.40 ± 3.35	77.83 ± 5.26	85.43 ± 2.36	87.21 ± 2.26	86.66 ± 2.01
H3K36me3_AM.immune		91.85 ± 0.93	92.75 ± 1.33	88.29 ± 6.18	92.61 ± 0.15	91.72 ± 0.09	90.60 ± 1.06	93.44 ± 0.70	93.89 ± 0.92
H3K36me3_TDH_ENCODE		56.10 ± 7.42	77.51 ± 0.29	75.57 ± 5.05	75.61 ± 6.73	73.16 ± 3.25	72.43 ± 9.49	73.28 ± 8.28	73.00 ± 8.69
H3K36me3_TDH immune		96.39 ± 1.96	87.78 ± 11.00	87.63 ± 0.32	90.13 ± 3.85	88.62 ± 8.01	95.67 ± 2.97	95.67 ± 2.97	95.67 ± 2.97
H3K36me3_TDH.other		77.00 ± 2.83	93.50 ± 2.12	79.00 ± 15.56	91.50 ± 0.71	70.50 ± 17.68	94.09 ± 2.28	94.09 ± 2.28	88.74 ± 5.28
H3K4me1_TDH_BP		78.63 ± 1.69	89.10 ± 2.37	87.02 ± 2.18	85.20 ± 1.68	89.43 ± 1.56	88.39 ± 1.63	88.79 ± 1.07	88.39 ± 1.63
H3K4me3_PGP immune		59.73 ± 5.00	71.79 ± 3.04	67.76 ± 3.35	70.11 ± 1.27	72.39 ± 0.45	70.68 ± 2.95	72.43 ± 1.89	73.55 ± 0.18
H3K4me3_TDH_ENCODE		92.33 ± 1.83	94.78 ± 1.04	95.37 ± 1.74	97.05 ± 1.26	93.89 ± 2.79	94.60 ± 1.62	94.94 ± 1.14	94.94 ± 1.14
H3K4me3_TDH immune		68.85 ± 1.39	71.79 ± 3.04	67.76 ± 3.35	70.11 ± 1.27	80.91 ± 3.16	80.61 ± 1.50	81.42 ± 1.50	81.98 ± 1.29
H3K4me3_TDH.other		85.15 ± 4.73	71.79 ± 3.04	67.76 ± 3.35	70.11 ± 1.27	91.83 ± 0.65	89.74 ± 1.76	90.16 ± 1.39	89.90 ± 1.99
H3K4me3_XJ.immune		67.13 ± 0.89	69.44 ± 4.29	71.89 ± 2.29	74.00 ± 3.64	71.98 ± 4.33	70.98 ± 2.36	72.29 ± 3.41	75.06 ± 2.40
H3K9me3_TDH_BP		48.94 ± 1.50	84.29 ± 1.75	85.94 ± 0.11	79.39 ± 6.81	84.19 ± 2.81	86.16 ± 1.43	85.04 ± 1.62	86.08 ± 2.48